and 32 for Kurinwas and 34, 34, 35, 36, 37, 42, 44, and 47 for the other sites.

17. M. R. Guariguata, R. L. Chazdon, J. S. Denslow, J. M. Dupuy, L. Anderson, *Plant Ecol.* **132**, 107 (1997).
18. R. L. Chazdon, R. K. Colwell, J. S. Denslow, M. R. Guariguata, in *Forest Biodiversity Research, Monitoring and Modeling: Conceptual Background and Old World Case Studies*, F. Dallmeier and J. Comiskey, Eds. (Parthenon, Paris, 1998), pp. 285–309.
19. M. Begon, J. L. Harper, C. R. Townsend, *Ecology* (Blackwell Science, Oxford, ed. 3, 1996).
20. J. H. Vandermeer, M. A. Mallona, D. Boucher, I. Perfecto, K. Yih, *J. Trop. Ecol.* **11**, 465 (1995).
21. In 1991, the proportions of stems that were pioneers were 0.05, 0.13, 0.17, and 0.19 for Bodega, La Unión, Loma de Mico, and Fonseca, respectively. In 1996, the corresponding figures were 0.09, 0.14, 0.15, and 0.16, respectively. Note that the order of sites ranging from farthest to nearest to the edge of the nondamaged forest (i.e., a potential source of pioneer seeds) is also Bodega, La Unión, Loma de Mico, Fonseca.
22. N. C. Garwood, D. P. Janos, N. Brokaw, *Science* **205**, 997 (1979).
23. P. J. Bellingham, E. V. J. Tanner, J. R. Healey, *J. Ecol.* **82**, 747 (1994).
24. T. C. Whitmore and D. F. R. P. Burslem, in *Dynamics of Tropical Communities*, D. M. Newbery, H. H. T. Prins, N. Brown, Eds. (Blackwell Science, Oxford, 1998), pp. 549–565.
25. K. E. Trenberth, *Current* **15**, 12 (1998).
26. M. C. Bove, J. B. Elsner, C. W. Landsea, X. Niu, J. J. O'Brien, *Bull. Am. Meteorol. Soc.* **79**, 2477 (1998).
27. We thank students from Universidad de las Regiones Autónomas de la Costa Caribeña de Nicaragua, Bluefields Indian Caribbean University, University of Central America, Hood College, University of Guelph, and University of Michigan for help in data collection; D. Goldberg for guidance on data analysis; and L. Curran, R. Burnham, and S. Levin for advice on the manuscript. The Centro de Investigaciones y Documentación de la Costa Atlántica (CIDCA) contributed logistic and intellectual support. Supported by NSF and the University of Michigan.

A Low Temperature Transfer of ALH84001 from Mars to Earth

Benjamin P. Weiss,[1]* Joseph L. Kirschvink,[1] Franz J. Baudenbacher,[2] Hojatollah Vali,[3] Nick T. Peters,[2] Francis A. Macdonald,[1] John P. Wikswo[2]

The ejection of material from Mars is thought to be caused by large impacts that would heat much of the ejecta to high temperatures. Images of the magnetic field of martian meteorite ALH84001 reveal a spatially heterogeneous pattern of magnetization associated with fractures and rock fragments. Heating the meteorite to 40°C reduces the intensity of some magnetic features, indicating that the interior of the rock has not been above this temperature since before its ejection from the surface of Mars. Because this temperature cannot sterilize most bacteria or eukarya, these data support the hypothesis that meteorites could transfer life between planets in the solar system.

Large-body impacts are the only known natural processes capable of ejecting a rock from Mars. It has been suggested that some rocks could be ejected without being shocked and heated (*1, 2*), and laboratory shock experiments have spalled lightly shocked material moving at about 20% of Mars' escape velocity (*3*). Thermal conductivity calculations (*4*) demonstrate that passage through Earth's atmosphere will not heat the interior of meteorites larger than ~0.3 cm above 100°C.

ALH84001 is a meteorite composed of ~95% orthopyroxene that accumulated in a magma chamber on Mars ~4.5 billion years ago (Ga) (*5*). Carbonate blebs, which may contain evidence for ancient life on Mars (*6*), formed in its fractures at about 4 Ga (*7*). During its first few billion years, ALH84001 experienced several shocks, probably from minor planet impacts (*8*). It was launched from the surface of Mars at ~15 million years ago by another impact (*9*) and after wandering through space, landed in Antarctica at about 11 thousand years ago (ka) (*10*).

Transmission electron microscopy imaging of the rims of the carbonate blebs in an ultrathin section prepared by focused ion beam detected single domain (SD) and superparamagnetic (SP) (*11*) magnetite (Fe_3O_4) and monoclinic pyrrhotite (Fe_7S_8) with characteristic lattice fringes. Because magnetic minerals have not been positively identified outside the carbonate bleb's rims, the blebs probably carry most of the magnetization in ALH84001. Other studies (*12*) have shown that this magnetite is stoichiometric (impurities <0.1%). After exposure to a 5-T field at room temperature, a 20-mg pyroxenite grain from ALH84001,236 containing multiple carbonate blebs exhibited a remanence transition at 112 K and a possible weaker remanence change at ~35 K, diagnostic of low-Ti magnetite ($Fe_{3-z}Ti_zO_4$ with $z < ~0.01$) and pyrrhotite, respectively. The grain's magnetization increased during cooling and then recovered ~90% of its original magnetization upon warming to room temperature, indicating the presence of SP and SD crystals and a lack of multidomain (MD) crystals. Anhysteretic remanent magnetization (ARM) and isothermal remanent magnetization (IRM) acquisition and demagnetization experiments on this grain also provide evidence of pyrrhotite (it acquires an IRM up to and beyond 1000 mT) and a small fraction of pseudo–single domain (PSD) crystals (alternating-field demagnetization is more effective at removing an IRM than an ARM). X-ray maps obtained by electron microprobe analysis detected Fe-sulfide crystals dispersed through the pyroxene matrix, suggesting that pyrrhotite may also be present outside the carbonate. We have thus detected two major magnetic minerals in ALH84001, located in the carbonate blebs and also probably in the pyroxene: magnetite and pyrrhotite ranging in size between SP, SD, and PSD. This confirms a previous identification of these magnetic minerals (*13*) and argues against the presence of titanomagnetite (*14*).

Kirschvink *et al.* (*13*) suggested that the interior of ALH84001 has been cooler than 110°C since before the formation of the carbonate. To obtain more precise thermal constraints, we imaged the perpendicular (east/west in the meteorite orientation system) component of the magnetic field of eight oriented slices of ALH84001 (*15*) using the Ultrahigh Resolution Scanning SQUID Microscope (UHRSSM). This magnetometer has a sensitivity of better than 0.1 nT and is capable of making two-dimensional images of the magnetic field of materials at room temperature with a resolution of 500 μm (*16*).

The fusion crust on the top-south surface of ALH84001,228b formed during its high-temperature passage through Earth's atmosphere and magnetic field, and is associated with an intense magnetic anomaly (Fig. 1). Moment magnetometry measurements of this and two additional samples with fusion crusts indicate that the meteorite initially came to rest in the ice with its east-southeast axis pointing up. Much weaker (~1% intensity) positive and negative magnetic features are present at distances of <5 mm in from the surface, implying that the heat pulse from atmospheric deceleration did not travel further than this into the meteorite. This shallow depth of heating is typical of most meteorites of this size (*4*). This suggests that the heterogeneous magnetization in the interior (Fig. 2) predates arrival at Earth.

Using the same technique, we made multiple magnetic images of ALH84001,232e, which was extracted from the interior of the

[1]Division of Geological and Planetary Sciences, 170-25, California Institute of Technology, Pasadena, CA 91125, USA. [2]Department of Physics and Astronomy, Vanderbilt University, 6301 Stevenson Center, Nashville, TN 37235, USA. [3]Electron Microscopy Centre, Department of Anatomy and Cell Biology and Department of Earth and Planetary Sciences, McGill University, 3640 University Street, Montreal QC H3A 2B2, Canada.

*To whom correspondence should be addressed. E-mail: bweiss@gps.caltech.edu

meteorite. The first image of the natural remanent magnetization (NRM) at room temperature (Fig. 2A) reveals a spatially heterogeneous pattern of magnetization like that observed in the interior portion of 228b. We also observed a similar, stable (17) pattern in UHRSSM images of four other cm-sized slices taken from the interior of the meteorite. Several positive (eastward) and negative (westward) features are present (black arrows), some of which are dipolar in character. The strongest of these is centered on a carbonate bleb containing magnetite and pyrrhotite located 100 μm below the surface of the slice. In some regions, the dipolar features are centered on fractures (Figs. 2 and 3), while elsewhere fractures form the boundary between pyroxene fragments that are magnetized in different directions. The latter has been observed in previous studies of individual ALH84001 grains (13, 14).

After producing the UHRSSM image of the NRM, slice 232e was then heated to 40°C for 10 min, cooled in an eastward 15-μT field, and then reimaged. It was then heated to 40°C for 10 min in a magnetically shielded furnace and cooled in a zero field (<10 nT) and reimaged. This cycle of heating and cooling was continued in 10° or 20°C steps up to 200°C. Oxidation of the iron-bearing phases was inhibited by first immersing the ALH84001 slices in mineral oil containing an organic antioxidant (α-tocopherol) and by re-

moving trapped air under vacuum before each heating cycle. Following the heating to 40°C, the magnitude of many magnetic features decreased (including the dipole centered on the carbonate) (Fig. 2, B and C) [first frame of Web fig. 1 (18)], completely erasing some that were present in the NRM scan (Fig. 2A). These features never regained the intensities present in the NRM image (Fig. 2C and Web fig. 1). At each temperature step above 40°C, different randomly oriented features weakened or strengthened in magnetization (Web fig. 1). The magnetization that unblocked at 40°C should have been mostly from pyrrhotite: our high-resolution transmission electron microscope (TEM) compositional maps showed that in the carbonate rims, magnetite is only two to three times more abundant than pyrrhotite and both minerals have similar crystal size distributions, while the theoretical range of pyrrhotite crystal sizes with blocking temperatures between room temperature and 40°C is ~1000 times larger than that of magnetite.

With rare exceptions, most rocks magnetize uniformly in the direction of the local magnetic field when they cool below their Curie temperatures or when their magnetic minerals crystallize out of a low-temperature solution. We conclude that ALH84001 should have been capable of isotropically acquiring a thermoremanent

magnetization (TRM) during our heating experiment and throughout its 4.5–billion year history (19). This conclusion is supported by two experiments. In the first, we subjected the large pyroxene grain studied by Kirschvink et al. (13) to three 100-mT magnetic pulses at room temperature to give the grain an IRM, which we measured after each pulse. After the first and second pulses, the grain was rotated 90° along the north and east directions, respectively, while keeping the field direction constant. In all three cases the magnetic phases in the grain remagnetized with the same intensity to within 1° of the field direction. In our second experiment, we compared the magnetization image obtained after heating to 200°C and cooling in the eastward 15-μT field with that obtained after heating to the same temperature and cooling in the zero field (Fig. 4). Almost the entire slice remagnetized in the eastward direction (20). Thus, if the meteorite was previously heated, many of the features that weakened after the laboratory heating to 40°C in the zero field (Fig. 2 and Web fig. 1) would have remagnetized isotropically and in the direction of the background field. Because the meteorite is even more likely to have isotropically acquired a TRM when it first cooled (i.e., before it had been shocked and deformed), it is also likely that the meteorite was originally magnetized in the direction of the local field.

At least three processes can have produced the spatial heterogeneity of the magnetization. The first is a brecciation event, in which fragments of the meteorite were rotated and translated with respect to one another without being heated to 40°C. Such an event could explain the association between the magnetization pattern and rock fragments (e.g., the clast on the left side of 232e in Figs. 2 and 3). The second process is the deposition of several generations of magnetic minerals over a period during which the relative orientation of the local magnetic field changed. The latter could explain the dipolar and other magnetic features centered on fractures (e.g., those centered on the dashed cracks in Fig. 2). A third process is a series of shock events, which could have heterogeneously heated the rock on submillimeter scales, selectively remagnetizing isolated regions in the rock. Treiman (8) has identified five shock deformational events and a carbonate formation event. The earliest deformation, which he labeled D1, mobilized and rotated fragments of the rock, forming mm-thick cataclastic granular bands. Later events (D2b and D3) produced brittle fracture surfaces that transect the granular bands (8). However, these events may have been too hot to produce a spatially heterogeneous
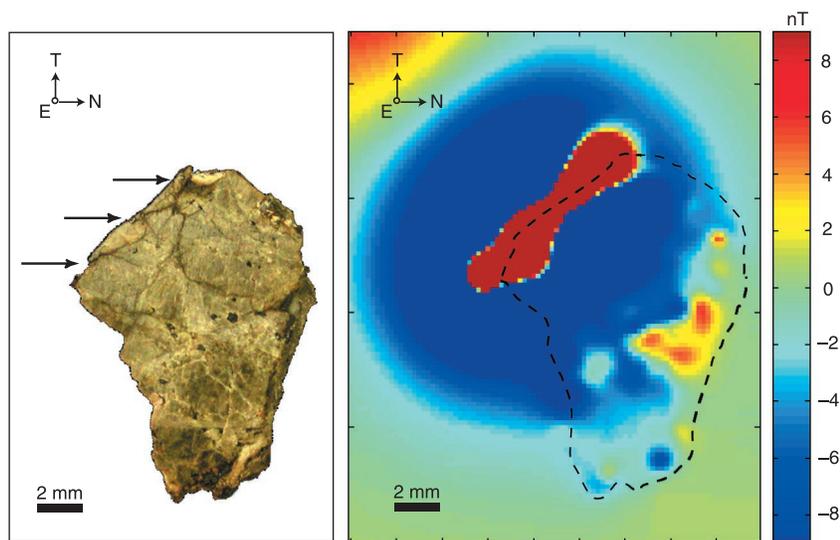

Fig. 1. (Left) Photograph of oriented slice ALH84001,228b that contains a small piece of the surface fusion crust (marked with arrows) oriented about normal to the image plane. This crust formed during entry through Earth's atmosphere. **(Right)** UHRSSM image of the same slice, displaying the east (out-of-the-page) component of the magnetic field at 250 μm above the slice. North is to the right and top is toward the top of the page, as demonstrated by the compass registered to the Johnson Space Center curatorial orientation system. An outline of the slice, corresponding to the edge of the slice in the photograph at left, is drawn around the sample. The color bar gives the field intensity in nT, with red and yellow (blue) corresponding to eastward (westward) magnetization. The fusion crust has been remagnetized by Earth's field in the east direction, with a peak intensity of ~1200 nT. A few millimeters toward the interior of the meteorite (i.e., to the lower right) the original heterogeneous pattern of magnetization is observable with amplitudes similar to those elsewhere inside the rock (Fig. 2). Scale bars, 2 mm.

magnetization (*8, 21*). The fractures from D1 and D2b were then partly filled with the magnetized carbonate blebs (event Cγ) and also phyllosilicates (*22*). We have correlated at least one dipolar feature centered over a crack with a carbonate bleb (Figs. 2 and 3). Some heterogeneity could also have been produced when the D3 event broke up and translated some of these carbonates (*8, 21*). A low-temperature D4 event also may have brecciated the meteorite late in its history (*8*).

Regardless of which particular event(s) are responsible for randomizing the magnetization, it is fairly certain that ALH84001 was not brecciated during or after its ejection from Mars. Such a brecciation is highly unlikely to occur for orbital dynamical reasons (*10, 23*). Furthermore, cosmic ray exposure studies demonstrate that ALH84001 was never shielded in a larger body in space (*24*). The latter indicates that the meteorite lacked appreciable self-gravity and so could not also have been broken up and reassembled during the ejection process. Although there is evidence that terrestrial water has flowed through the meteorite (*25, 26*), the carbonates and their associated magnetic minerals originated on Mars (*6*). It is unlikely that significant quantities of magnetic minerals were deposited in ALH84001 while on Earth, because the meteorite was mostly encased in ice in subzero temperatures and no secondary minerals have been identified other than those from Mars (*8, 22*).

Using recently measured magnetization parameters (*27*), we calculated a Pullaiah diagram (*28*) for monoclinic pyrrhotite, which gives the time required for an SD crystal to magnetize (in the presence of a field) or demagnetize (in zero field) at a given temperature (Web fig. 2). Although the diagram is not always a reliable indicator of the behavior of natural crystal assemblages (*29*), it nevertheless suggests that any viscous remanent magnetism (VRM) acquired by ALH84001 while in Antarctica is unlikely to have affected pyrrhotite crystals with 10-min blocking temperatures of 40°C and above (*30*).

The impactors capable of removing rocks from Mars, which are likely several km in diameter (*23*) and moving at a Keplerian velocity of ~10 km s^{-1}, would produce a shock pulse of duration ~0.1 s (*31*) during collision with the martian surface. The duration of thermodynamically irreversible heating produced during this process can be orders of magnitude larger than this shock pulse time (*31*). The Pullaiah diagram demonstrates that crystals that magnetize after heating to 40°C for 10 min would magnetize after heating to 125°C for >10^{-4} s or to 60°C for >1 s. Thus, if during its ejection, ALH84001 had been heated to 40°C and then cooled in a zero

field, no magnetic features would have changed in intensity during our 10-min heating experiment. If the meteorite had been heated to 40°C and instead cooled in a nonzero field, features magnetized in only one of the two directions would have weak-
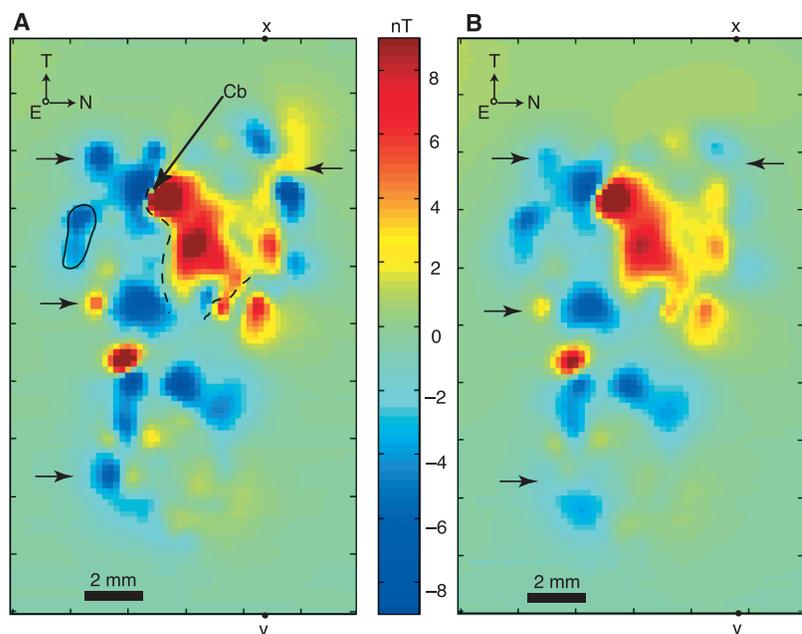

Fig. 2. UHRSSM images of oriented slice ALH84001,232e. (**A**) NRM of the sample at room temperature before heating. Fracture surfaces on which two dipolar features sit are labeled with dashed lines. A fracture defining a distinctly magnetized grain is labeled with a solid line. A carbonate bleb containing magnetite and pyrrhotite was found 100 μm below the surface at the location labeled "Cb." (**B**) Magnetization of the sample after being heated to 40°C for 10 min. The arrows in (A) and (B) indicate features that show significant decrease in intensity. Scale bars represent 2 mm and the color bar is in nT. (**C**) Magnetic intensity variations along a line connecting points x and y, as observed in the unheated sample and after heating to 40° and 200°C. This is a three-column running average centered on the line of pixels joining x and y.
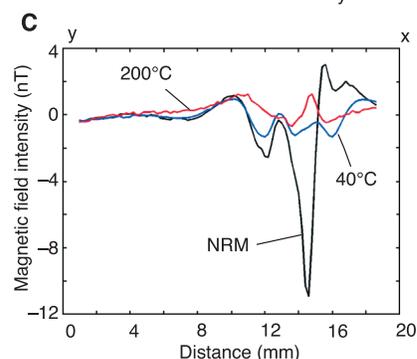

Fig. 3. Backscattered scanning electron microscopy image of top half of oriented slice ALH84001,232e, showing fractures (dark black lines), orthopyroxene (light gray), feldspathic glass (dark gray), and chromite (white). Both fractures labeled as dashes lines in Fig. 2A are visible and identified by a set of arrows. In one of them, a carbonate bleb containing magnetite and pyrrhotite was found 100 μm below the surface at the location labeled "Cb" (as in Fig. 2A). The carbonate bleb was observed after removal of a 100-μm-thick layer from the original surface from which the magnetic map was obtained. The uniformly magnetized clast (defined by solid line in Fig. 2A) is visible at left. Scale bar, 1 mm.
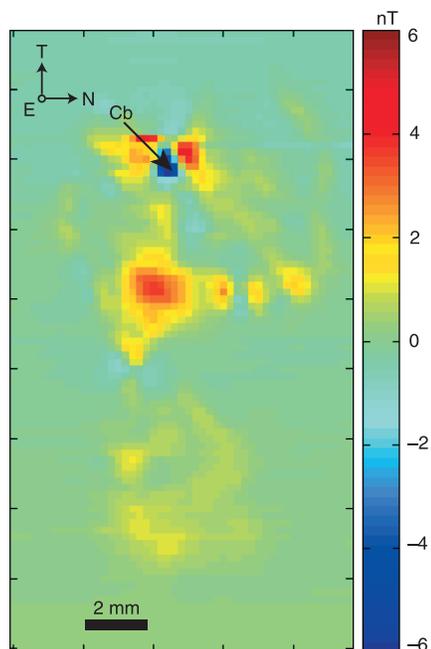
Fig. 4. Intensity difference between spatially registered UHRSSM images of oriented slice ALH84001,232e after heating to 200°C: image taken after cooling in an eastward 15 μT minus image taken after cooling in a zero field. Prior to subtraction, images were registered by maximizing their cross-correlation. The carbonate bleb identified in Figs. 2 and 3 is also labeled here ("Cb"). Scale bar, 2 mm. The background intensity gradient in the vertical direction is an artifact from instrument drift.

ened during our experiment, while the oppositely magnetized features strengthened. Because eastward and westward features (i) weakened by as much as 100% during demagnetization at temperature steps between 40° and 200°C and (ii) ALH84001 magnetizes isotropically in the direction of an applied field, ALH84001 has most likely not been heated even to 40°C since before it left Mars.

This means that ALH84001 was only lightly shocked during its ejection (*1, 2*) and therefore originates from near the planet's surface. Our data support recent suggestions (*32, 33*) that shock-implanted gases in ALH84001 did not enter the meteorite during ejection, but instead sample a martian atmosphere that is much older than 15 million years. Our results also indicate that major impact events are capable of moving rocks from the surface of Mars to the surface of Earth without subjecting them to temperatures high enough to cause thermal sterilization of eukarya or bacteria. Dynamic simulations of martian impact events (*2, 10, 23, 34*) indicate that materials can be launched into a wide variety of orbits. Although most of the ~1 ton of martian rocks which land on Earth each year have spent several million years in space, one in 10^7 of the arriving rocks will

have made the journey in less than a year (*23*). Every million years, ~10 rocks larger than 100 g are transferred in just 2 to 3 years (*23*). Bacterial spores, as well as microorganisms within rocks, can survive in deep space for more than 5 years (*35*). These results indicate that it may not be necessary to protect Earth's present biosphere by quarantining rocks retrieved by a Mars sample return mission (*36*). Conditions are appropriate to allow low-temperature rocks—and, if present, microorganisms—from Mars to be transported to Earth throughout most of geological time.

References and Notes
1. H. J. Melosh, *Nature* **332**, 687 (1988).
2. H. J. Melosh, *Nature* **363**, 498 (1993).
3. A. J. Gratz, W. J. Nellis, N. A. Hinsey, *Nature* **363**, 522 (1993).
4. V. A. Bronshten, *Physics of Meteoric Phenomena* (Kluwer Academic, Boston, 1983).
5. L. E. Nyquist, B. Bansal, H. Wiesmann, C.-Y. Shih, *Lunar Planet. Sci.* **XXVI**, abstract 1065 (1995).
6. D. S. McKay *et al.*, *Science* **273**, 924 (1996).
7. L. E. Borg *et al.*, *Science* **286**, 90 (1999).
8. A. H. Treiman, *Meteorit. Planet. Sci.* **33**, 753 (1998).
9. T. D. Swindle, J. A. Grier, M. K. Burkland, *Geochim. Cosmochim. Acta* **59**, 793 (1995).
10. B. J. Gladman, J. A. Burns, M. Duncan, P. Lee, H. F. Levison, *Science* **271**, 1387 (1996).
11. Unlike SD grains, SP grains are too small to hold a stable magnetization at room temperature. MD grains are so large that they contain several magnetic domains, while PSD grains are sized between SD and MD and exhibit intermediate behavior. NRM is the magnetization that is observed in a rock prior to laboratory treatment. It can take the form of TRM, produced when a crystal cools below its blocking temperature in the presence of a magnetic field. The blocking temperature is defined as the temperature at which a ferromagnetic crystal is able to hold a directionally stable magnetization. The highest possible blocking temperature is the Curie point. IRM can be acquired during short exposure to strong magnetic fields at constant temperature. ARM is acquired during exposure to an alternating field superimposed on a constant bias field. VRM can be accumulated during long exposures to ambient magnetic fields; its presence is usually indicative of MD or SP crystals.
12. K. L. Thomas-Keprta *et al.*, *Geochim. Cosmochim. Acta*, in press.
13. J. L. Kirschvink, A. T. Maine, H. Vali, *Science* **275**, 1629 (1997).
14. D. W. Collinson, *Meteorit. Planet. Sci.* **32**, 803 (1997).
15. This relative orientation was done using the fine sawblade striations left on the original flat surface cut at the Johnson Space Center (Houston, TX) during the sampling of the meteorite. In a class-1000 magnetically shielded clean lab at the California Institute of Technology (Caltech), these oriented fragments were cemented onto standard Pyrex microscope slides using cyanoacrylate cement, and cut in Nanopure water with a 25-μm-diameter diamond-impregnated continuous loop wire saw into a series of slices ~1 to 2 mm thick. Surfaces were then smoothed using wet 40-mesh diamond polishing paper. Each slice retained the relative orientation of the initial subsample, and was given a letter designation (e.g., 232a, 232b, 232c, etc.) in order of increasing distance from the original saw-cut surface. Because of visible metallic contamination and possible local heating from the original diamond-saw cut in Houston, we did not use the "a" sections in our magnetic imaging studies. Any shock remanent magnetization (SRM) from the sampling process should not have remagnetized the crystals (coercivity ~60 mT) which unblocked during our heating experiments described later, and could not have produced the multidirec-

tional magnetization pattern that persists after heating to more than 200°C.
16. The UHRSSM is reported in F. J. Baudenbacher, N. T. Peters, J. P. Wikswo, M. Radparvar [*Bull. Am. Phys. Soc.* **44**, 702 (1999)] and F. Baudenbacher, N. Peters, J. P. Wikswo [*Bull. Am. Phys. Soc.* **45**, 651 (2000)]. The general techniques of scanning superconducting quantum interference device (SQUID) microscopy are reviewed by J. P. Wikswo Jr. [in *SQUID Sensors: Fundamentals, Fabrication and Applications*, H. Weinstock, Ed. (Kluwer Academic, Amsterdam, 1996), pp. 307–360] and J. R. Kirtley, J. P. Wikswo Jr. [*Annu. Rev. Mater. Sci.* **29**, 117 (1999)]. The application of SQUID imaging to geophysical samples was first demonstrated in I. M. Thomas, T. C. Moyer, J. P. Wikswo Jr. [*Geophys. Res. Lett.* **19**, 2139 (1992)]. The UHRSSM which produced our data employed a 500-μm-diameter superconducting NbTi pickup coil wound on a sapphire bobbin and held at 4.2 K. The coil is located in the vacuum space of the cryostat separated by a 25-μm-thick sapphire window from the room-temperature ALH84001 samples, with a distance of ~250 μm between the coil and sample. Scans were made in a grid of 200-μm steps in a magnetically shielded room.
17. In a second UHRSSM image of one of these slices taken 3 months later, the previously observed magnetization did not detectably change in pattern or intensity. This gives strong evidence that VRM and MD crystals are not playing an important part in the observed magnetization.
18. Supplementary figures are available at www.sciencemag.org/feature/data/1051805.shl
19. The few known examples of rocks that acquire a TRM that varies in direction within the sample are those with strong magnetic anisotropy and/or self-reversing tendencies (*29*). Neither of these properties should be present in ALH84001. Although individual crystals can exhibit magnetocrystalline or shape anisotropy, this could not effect the gross magnetization of cumulates like ALH84001 in which the crystals are randomly oriented. Highly foliated rocks can acquire magnetic anisotropy due to alignment of the crystals, although this has not been noted for the heavily shocked Apollo samples (*37*). Four mechanisms of self-reversed magnetization (magnetization in a direction opposite that of other nearby grains and the background field) have been reported (*29*). Three of these are only known to occur in the presence of high-Ti iron oxides (*29*), none of which have been identified in ALH84001 (*12*). The fourth has been observed in large MD synthetic magnetic grains with exsolved magnetic minerals, but has never been conclusively identified in natural samples (*29, 38, 39*). It is unlikely to occur in ALH84001, which contains PSD and smaller crystals and lacks detectable exsolution features in any minerals (*40*).
20. The region that appears to be westwardly magnetizing (at the top center of Fig. 4) is centered on a carbonate bleb (Fig. 3). Its presence does not require that the rock has magnetic anisotropy or is self-reversing. If the field in which the meteorite acquired its NRM was less than 15 μT, then westwardly magnetized regions could increase after laboratory heating at low temperatures since the newly acquired magnetization, although pointing eastward, is also higher in intensity. This could explain some of the apparent anisotropy. Some of this apparent anisotropy is also likely to be an artifact resulting from pixelation noise, imperfect registration of the subtracted images, and most importantly, differences in heating and cooling time between the zero field and 15-μT field steps. Because the westwardly magnetizing region is much more strongly magnetized than the rest of the slice, the differences in heating and cooling time will affect this feature more strongly.
21. C. K. Shearer, L. A. Leshin, C. T. Adcock, *Meteorit. Planet. Sci.* **34**, 331 (1999).
22. A. J. Brearley, *Lunar Planet. Sci.* **XXXI**, abstract 1203 (2000).
23. B. Gladman, *Icarus* **130**, 228 (1997).
24. J. N. Goswami, N. Sinha, S. V. S. Murty, R. K. Mohapatra, C. J. Clement, *Meteorit. Planet. Sci.* **32**, 91 (1997).

25. J. L. Bada, D. P. Glavin, G. D. McDonald, L. Becker, *Science* **279**, 362 (1998).
26. N. Sugiura, H. Hoshino, *Meteorit. Planet. Sci.* **35**, 373 (2000).
27. A. Menyeh, W. O'Reilly, *Phys. Earth Planet. Inter.* **89**, 51 (1995).
28. G. Pullaiah, G. Irving, K. L. Buchan, D. J. Dunlop, *Earth Planet. Sci. Lett.* **28**, 133 (1975).
29. D. J. Dunlop, O. Ozdemir, *Rock Magnetism: Fundamentals and Frontiers* (Cambridge Univ. Press, New York, 1997).
30. According to the diagram (Web fig. 2), during ALH84001's 2-year stay in the Caltech shielded room before the start of our experiments, all crystals with 10-min blocking temperatures below ~50°C could have unblocked. This would seem to include any VRM acquired while in Antarctica and SRM from sample preparation, as well as the magnetization that unblocked during our 40°C heating step (Fig. 2 and Web fig. 1). The diagram also suggests that residence at the Johnson Space Center may have remagnetized crystals with 10-min blocking temperatures below ~65°C. Passage through the low-field (several nT) environment between Mars and Earth is unlikely to have left a VRM, but may have demagnetized crystals with 10-min blocking temperatures below ~80°C (Web fig. 2). On the other hand, the diagram (Web fig. 2) is untested and required extrapolation of a coercivity function that was measured on temperatures only down to 20°C and on crystals (sized 100 nm to 30 μm) larger than those in the diagram (41). The Pullaiah diagram for magnetite has disagreed by several orders of magnitude with other theoretical treatments as well as some experiments (29). Most importantly, ALH84001 thermally demagnetizes steadily and in a spatially heterogeneous manner from 40° to 200°C (Web fig. 1). Because this a more trustworthy indicator of the lack of VRM, the magnetization that unblocked during the 40°C heating step was probably acquired while on Mars. Nevertheless, if the diagram (Web fig. 2) is taken as correct, then in the most stringent scenario (that ALH84001 spent several My at 5°C while in space, such that all grains with 10-min blocking temperatures below 80°C were remagnetized) the thermal constraint on ALH84001 since before ejection would become 80°C.
31. H. J. Melosh, *Impact Cratering: A Geologic Process* (Oxford Univ. Press, Oxford, 1986).
32. D. D. Bogard, D. H. Garrison, *Meteorit. Planet. Sci.* **34**, 451 (1999).
33. J. D. Gilmour, J. A. Whitby, G. Turner, *Geochim. Cosmochim. Acta* **62**, 2555 (1998).
34. B. J. Gladman, J. A. Burns, *Science* **274**, 161 (1996).
35. G. Horneck, H. Bucker, G. Reitz, *Adv. Space Res.* **14**, 41 (1994).
36. B. E. Digregorio, G. V. Levin, P. A. Straat, *Mars: The Living Planet* (Frog Ltd., Berkeley, CA, 1997).
37. M. Fuller, S. M. Cisowski, in *Geomagnetism*, J. A. Jacobs, Ed. (Academic Press, Orlando, FL, 1987), vol. 2, pp. 307–455.
38. K. Zapletal, *Phys. Earth Planet. Inter.* **70**, 302 (1992).
39. M. Bina, L. Daly, *Phys. Earth Planet. Inter.* **85**, 83 (1994).
40. A. H. Treiman, *Lunar Planet. Sci.* **XXXI**, abstract 1225 (2000).
41. A. Menyeh, W. O'Reilly, *J. Geophys. Res.* **101**, 25045 (1996).

Impacts of Climatic Change and Fishing on Pacific Salmon Abundance Over the Past 300 Years

Bruce P. Finney,[1]* Irene Gregory-Eaves,[2] Jon Sweetman,[1] Marianne S. V. Douglas,[3] John P. Smol[2]

The effects of climate variability on Pacific salmon abundance are uncertain because historical records are short and are complicated by commercial harvesting and habitat alteration. We use lake sediment records of $\delta^{15}N$ and biological indicators to reconstruct sockeye salmon abundance in the Bristol Bay and Kodiak Island regions of Alaska over the past 300 years. Marked shifts in populations occurred over decades during this period, and some pronounced changes appear to be related to climatic change. Variations in salmon returns due to climate or harvesting can have strong impacts on sockeye nursery lake productivity in systems where adult salmon carcasses are important nutrient sources.

Historical records of air and ocean temperature, as well as atmospheric pressure fields, show significant interdecadal fluctuations in the North Pacific region (1–3). These climatic fluctuations appear to have had large impacts on marine ecosystems (1, 3–5). Salmon catch records suggest a correlation between the intensification of the Aleutian Low, increased coastal sea surface temperatures in the eastern North Pacific, and increased production of Alaskan salmon during the 20th century (6). However, the historical record is of insufficient length or quality to assess the representativeness of these recent observations. Because Pacific salmon are important economic and cultural resources, their viability in response to future climatic change is of great concern (7). Here, we present high-resolution records of diatoms, cladocerans, and sedimentary $\delta^{15}N$ to explore the sockeye salmon–climate connection over the last ~300 years in sockeye nursery lakes located on western Kodiak Island and near Bristol Bay, Alaska.

Sockeye salmon (*Oncorhynchus nerka*) typically spend 2 to 3 years feeding in the North Pacific and subsequently migrate to their home lake–stream system where they spawn and die. Sockeye often return in tremendous numbers, and it is not uncommon for densities to reach the equivalent of 5000 to 30,000 adult fish (average weight ~2.7 kg) per km² of lake surface area (8). After hatching, juvenile sockeye spend 1 to 3 years in their home nursery lake feeding primarily on pelagic zooplankton; however, >99% of the biomass of adult sockeye is accumulated in the marine environment (8). Therefore, the nutrients originating from carcasses of post-spawning adults are almost exclusively of marine origin. These carcass-derived nutrients are often significant sources of nutrients to these oligotrophic systems (9). For example, in Karluk Lake, Kodiak Island (Fig. 1), carcass-derived nutrients typically contribute more than half of the lake-water phosphorus (P) and nitrogen (N) annually (10). Atmospheric and anthropogenic inputs to the lakes we studied are insignificant (10); the catchments are virtually undisturbed by human activities, and many are not forested, thus reducing the confounding effects of forest fires.

Adult sockeye salmon carcasses have high $\delta^{15}N$ (~12‰) relative to terrestrial N in Alaskan nursery lakes, which typically have values close to atmospheric levels (0‰) (11). Stable N isotopes thus can be used to track the salmon-derived N into the biota of freshwater and terrestrial ecosystems (11–13). In the lakes we studied, there is a strong association between zooplankton $\delta^{15}N$ and salmon-derived nutrient (SDN) loading (Fig. 2A). These nutrients are subsequently transferred to higher trophic levels, as demonstrated by the relation between juvenile sockeye salmon $\delta^{15}N$ and the SDN loading in their nursery lakes (Fig. 2B). Lake sediments faithfully archive this information, as shown by the relation between surface sediment $\delta^{15}N$ and SDN loading (Fig. 2C). Factors known to influence sedimentary $\delta^{15}N$ in other settings

[1]Institute of Marine Science, University of Alaska Fairbanks, Fairbanks, AK 99775, USA. [2]Paleoecological Environmental Assessment and Research Lab (PEARL), Department of Biology, Queen's University, Kingston, Ontario K7L 3N6, Canada. [3]Department of Geology, University of Toronto, 22 Russell Street, Toronto, Ontario M5S 3B1, Canada.

*To whom correspondence should be addressed. E-mail: finney@ims.uaf.edu